Optical Tweezer Trapping of Colloidal Polystyrene and Silica Microspheres

Including calibration, force measurements, and preliminary surface charge experiments

By

Kyle C. Peters

An Undergraduate Thesis Submitted to
Oregon State University

In partial fulfillment for the degree of

Baccalaureate of Science in
Physics

Spring 2013

Abstract

Optical trapping is a tool used throughout a wide variety of disciplines ranging from precisely probing and manipulating sub-micron organisms in biology to analyzing fundamental charge transfer in colloidal physics. This thesis presents research involving optical tweezer force measurements of polystyrene and silica microspheres. In addition, preliminary work in tweezer-based surface charge measurements is developed to examine surface charge at the solid-liquid interface of silica microspheres.

The main purpose of constructing, and testing the tweezer apparatus is to utilize its trapping capability for experiments involving charge measurements. The optical tweezer related research provides information pertaining to force measurements of a single beam optical tweezer trap equipped with an independent back focal-plane laser position detection system. Calibration methods and experimental power dependence for $1\mu m$-diameter polystyrene and silica microspheres provide proof-of-principle results that exhibit expected linear power dependence to within an experimental error of 10.5%.

The research involving charge measurements provide preliminary the framework for studying charging/discharging dynamics of $1\mu m$-diameter colloidal silica spheres. Studying (dis)charging dynamics on nano-scale levels is difficult, however, the methods presented in this thesis uses an ultrasensitive technique adopted from Roberts *et al.*[1] to measure the effective surface charge of particles dispersed in water. This is performed by conducting

[1]G Seth Roberts, Tiffany A Wood, William J Frith, and Paul Bartlett. Direct measurement of the effective charge in nonpolar suspensions by optical tracking of single particles. The Journal of chemical physics, 126(19):194503–194503, 2007.

electrophoresis experiments designed to track the movement of an optically trapped particle in the presence of an applied (AC) electric-field. Experimental results demonstrate the ability to measure the effective surface charge. The proof-of-principle experiments show that for a $1\mu m$ silica microsphere the surface charge is found to be in the range of $66q_{el} - 113q_{el}$, as compared to Roberts *et al.* nonpolar suspended PMMA particles $14q_{el}$, yet similar to Behrens *et al.*[2] measurements of silica in deionized water $471q_{el} - 2200q_{el}$.

The preliminary work documented in this thesis sets forth the necessary groundwork to examine charging dynamics of molecular-coated silica microspheres, and further experiments are being designed to study ADT-TES-F coatings at varying electric-field frequencies.

[2]S. H. Behrens and D. G. Grier. The charge of glass and silica surfaces. Journal of chemical physics, 115(14):6716–6721, 2001.

Acknowledgements

I owe my deepest gratitude to my advisor Oksana Ostroverkhova for her support, guidance, and patience throughout my first research experience. I am grateful, and honored to have been provided with this opportunity.

Many thanks to the OPE members both current and former, in particular the short, but insightful guidance of Mark Kendrick, and Rebecca Grollman who shared with me the agony and excitement of experimental physics.

Finally, thanks to my family for all the support, instilling in me confidence and motivation to pursue my studies in physics.

This project was partially funded by the National Science Foundation.

Contents

List of Figures

List of Tables

Chapter 1

Introduction

The interaction of light with matter is a fundamental method commonly used in research as a tool to manipulate and analyze properties of materials. Research exploring organic optical materials, as opposed to inorganic, is of interest due to their low cost and the ability to tune particular properties by synthetic modifications [1]. Slight alterations can change optical, structural, and electrical properties. These modifications can provide enhancements tailored for particular applications in solar cells, thin-film transistors, and light-emitting diodes (LED) [2, 3]. This thesis consists of (1) the experimental design, development, and testing of a single-beam optical tweezer trap that utilizes a separate laser-based position detection scheme, and (2) preliminary work in conducting optical tweezer-based surface charge measurements of silica microspheres.

1.1 Optical Tweezer Overview

Optical tweezer traps provide the ability to manipulate and measure picoNewton forces of sub-micron dielectric particles. Tweezer traps are produced by taking advantage of radiation pressure. Ashkin [4] first discovered that a tightly focused laser beam could accelerate microparticles, and by arranging two counterpropagation lasers, focused at the same spot, had the

ability to confine a particle in three dimensions. From this research he identified the radiation pressure to be the central criterion in the technique of optical trapping and sub-micron particle manipulation.

Contemporary optical tweezers have been commonly used throughout the experimental field of physics, chemistry, and biology due in part by their capability to confine, manipulate, and apply picoNewton forces on sub-micron particles [5]. Having the ability to move particles in the realm of nanometers and apply small force free from optical damage has been particularly useful in the study of biological systems [6]. Recently, optically trapped charged particles have been used as force probes to map electric fields generated by microelectrodes and to measure effective surface charge [7, 8, 9].

The work in optical trapping presented in this thesis is similar to the applications above, in that an optical tweezer apparatus is constructed, tested, and used for experiments to explore charge carrier dynamics of organic molecules. The optical trapping portion of this thesis is presented as follows: Chapter 2 presents and overview of optical trapping theory, including the Mie (2.1) and Rayleigh (2.2) regime. Chapter 3 describes the optical tweezer setup (3.1) and sample cell preparation (3.2). Chapter 4 describes the model (4.2), and analysis (4.3) involved in particle trapping. Chapter 5 describes the calibration process and the factors involved. Chapter 6 presents optical trapping experiments, including power dependence (6.2), sphere-to-sphere variation (6.3), and sample depth dependence measurements (6.4).

1.2 Surface Charge Measurement Overview

Understanding how molecules donate and accept charge is an important aspect in (opto)electronic applications. The OPE group at Oregon State University have been utilizing single-molecule fluorescence spectroscopy to studying intermolecular interactions of organic molecules. In particular, functionalized anthradithiophene (ADT) with triethylsilylethynyl (TES) side-groups and fluorinated (F) end-groups (ADT-TES-F). However, optical tweezer-

based charge measurements may provide an alternative approach to analyze charging dynamics of specific organic molecules. This type of application involving tweezer trapping is relatively new, therein lies potential for improvement and sophistications that may provide detailed information about mechanisms involved in (dis)charging dynamics at sub-micron scale.

Within recent years, highly sensitive techniques involving optical tweezers have been developed to investigate the surface charge carried on isolated dielectric microparticles in nonpolar liquid with elementary charge (q_{el}) resolution [8, 9, 10]. Studying charge transfer on the nanometer scale requires extremely precise measurements that are particularly challenging in practice. Surface charge measurements are most readily performed through electrophoresis experiments, that is, measuring a particle's position in the presence of an applied (AC) electric-field.

Preliminary research involving surface charge measurements presented in this thesis is similar to the work of Roberts *et al.* [8]. In that, the methods described in [8] will be used to measure the effective surface charge carried on $1\mu m$-diameter silica microsphere suspended in water. The results are compared to the known surface charge for silica microspheres and serve as a control in further experiments.

Research involving optical tweezer-based electrophoresis experiments in Chapter 7 are outlined as followed: Section 7.1 explores the model and basic principles governing electrophoresis experiments. Section 7.2 covers the preliminary work in electrophoresis experiments, including sample cell preparation, modifications (7.2), and (AC) electric-filed frequency dependent measurements on silica microspheres (7.2.1), followed by the results and discussion(7.2.1).

Chapter 2

Principles of Optical Trapping

Optical trapping and manipulation of dielectric particles has been achieved throughout a vast range of particle size from nanometers to hundreds of micrometers. As a consequence of differing length scales there is no single theory, or model, accurately describing this scale range. As a result, two regimes are traditionally used to describe the optical forces of trapping for conflicting particle length scales relative to the trapping laser wavelength λ. When the target particle diameter d is much larger than the trapping wavelength ($d \gg \lambda$) the conditions for *Mie scattering* are satisfied. In such cases, a simple ray optics model can be used to within a good approximation for most trapping applications. For particles much smaller than the trapping wavelength ($d \ll \lambda$) the conditions for *Rayleigh scattering* are satisfied, and electromagnetic theory can be used by treating the particle as a point dipole [11, 12, 13].

2.1 Geometric (ray) Optics Model: Mie Regime ($d \gg \lambda$)

Particle trapping within the Mie regime originates from the transfer of momentum between the incident laser beam and the particle surface through a

scattering process [14]. When a transparent dielectric microsphere is near the beam-focus it experiences forces due to constant bombardment of photons. This process is denoted as radiation pressure [4, 11]. Impinging photons on the surface of the particle are traditionally decomposed into two contributing force components: (1) **scattering forces** ($\vec{F}_{scat}$), and (2) **gradient forces** ($\vec{F}_{grad}$). This *traditional*[1] model is simply an intuitive approach to examine the complete optical force contributions as a whole [12].

The scattering forces ($\vec{F}_{scat}$) can be thought of as an infinite stream (ray) of photons striking the particle surface. Since photons have momentum, each interaction exerts a force which tends to push the particle away from the beam focus. As a result, **the scattering force acts in the direction of light propagation and is proportional to the incident laser intensity**.

For most situations incident light intensity is distributed uniformly, in which case the scattering force dominates. However, in the case of a steep intensity gradient, such as one produced at the focal point, the gradient force component ($\vec{F}_{grad}$) contributes largely to the overall optical forces acting on an object. The transmitted light is refracted, resulting in a change of momentum as it enters and exits the particle. The gradient forces ($\vec{F}_{grad}$) arise from Newton's three law, the refracted light momenta transfer between particle surface and its surrounding medium. Thus, **the gradient force acts in the direction of the focal point and is proportional to the gradient of the laser intensity** hence the *gradient* force.

2.2 Rayleigh Regime ($d \ll \lambda$)

In general, the criteria for Rayleigh scattering theory is that the particle is smaller than $\lambda/20$ (d$\ll\lambda$) [16]. Within the Rayleigh regime the incident laser light cannot be represented by an infinite number of rays. Instead, the spherical particle is considered a point dipole that scatters light [13, 14].

[1] The traditional approach is an approximation which neglects the contributions of absorption forces ($\vec{F}_{abs}$), for further information regarding this force see Ref. [15, 12]

The gradient force ($\vec{F}_{grad}$) arise from the interaction between the inhomogeneous electric-field of the trapping laser and the dielectric particle material[2]. Unlike conductors, dielectrics are composed of atoms with tightly attached electrons to their respected nuclei, thus within the presence of an external electric-field, electrons are unable to roam about the material, as is true for electrons in conductors. However, the tightly attached electrons (within their respective orbital cloud) can change orientation direction (shift or rotate) within the bounds of their respected atom or molecule [17]. When placed in an inhomogeneous electric-field (the laser focus) the individual atoms can be thought of as tiny dipoles that align to the direction of the electric-field. The polarization alignment, and fluctuation imposed by the field yield a force on each dipole in the direction of highest intensity (laser focus). Thus, for dielectric particles **the gradient force is proportional to the intensity gradient at the focus and the particles polarization** [12, 17]. It is within this interaction between the dipoles and the electric-field fluctuations, near the focus, that creates the gradient *restoring* force. A pictorial description of this interaction is illustrated in Figure 2.1.

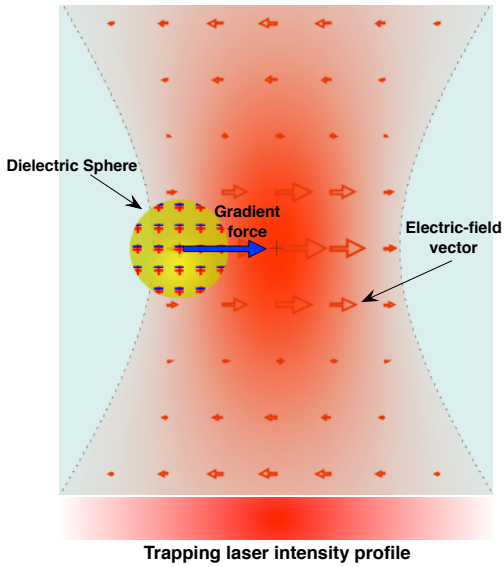

Figure 2.1: Induced dipole depiction of the gradient force acting on a dielectric microsphere near the trapping laser's diffraction-limited focus. Illustration was generated through Ref. [18].

Figure 2.1 depicts the gradient force vector ($\vec{F}_{grad}$) that arises from in-

[2]Laser light is usually linear-polarized in a particular orientation orthogonal to the direction of propagation. The polarization (direction of E-field) alternates sinusoidally thus changing from positive to negative, and back to positive in one wavelength-time

duced dipoles within a dielectric microsphere near the center of an optical trap. For this particular snapshot in time the intensity gradient causes the force pulling all the positive dipole ends towards the right to be greater than the negative dipole ends pulling to the left. At a later time when the electric-field switches direction each dipole will also shift slightly in orientation, as above, resulting in a net force pointing toward the center of the laser focus.

To generate a stable three dimensional trap, the axial ($\hat{z}$) components of the gradient force pulling the particle towards the focus must overcome the scattering components pushing the particle away from the focus. In order to satisfy this condition, the trapping laser must exhibit a steep intensity gradient at the focus. This condition can be achieved by using a high numerical aperture (N_A) microscope objective that tightly focuses the trapping laser down to a diffraction-limited spot [12]. Oil immersed objectives ($\mathrm{N}_A \approx 1.26$) are commonly used in particle trapping applications due to their ability to gain a near diffraction-limited focus without sacrificing trapping power at increased depth.

Chapter 3

Optical Tweezer Design and Construction

Optical tweezers are typically used to apply or measure small forces and displacements of sub-micron dielectric particles. This type of instrument is designed to be highly sensitive, allowing measurements on the order of picoNewtons and nanometers. The basic components of any optical tweezer instrument is merely a trapping laser, basic beam steering (mirrors), expansion (lenses), and filtration devices. A high numerical aperture (NA) objective, condenser, and some sort of detection or monitoring system are required to track the specimen's movement.

The instrument constructed in this research thesis is a single-beam gradient-force optical tweezer trap that utilizes a separate laser-based position detection system (Figure 3.1). The optical trap is a reconstruction of Mark Kendrick's optical trap previously built in 2007[1] with slight modifications.

[1]See Ref. [13, 15] for alternative information involving the construction.

3.1 Optical Tweezer Setup

The tweezer trap depicted in Figure 3.1 is constructed around a custom inverted microscope that is equipped with an oil immersed objective (Edmund Optics, 100X, NA 1.26, 160 mm tube length), which collects and tightly focuses inbound laser light. A beam expansion lens pair (L2 & L4) is used to overfill the objective's back aperture, while mirrors (M1 & M2) are adjusted to steer the beam over the aperture. A lower powered Helium-Neon (He-Ne) detection laser (633nm) is also expanded to overfill the back aperture (L3 & L4). L3 is mounted on an adjustable x-y-z-plane stage, which is used to adjust the detection laser focal plane.

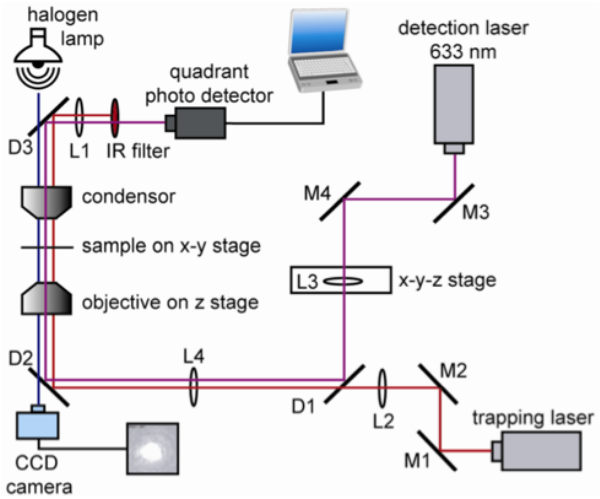

Figure 3.1: Experimental setup, which includes an inverted microscope arrangement (objective and condenser) to highly focus laser light within the trapping plane to trap particles. Schematic taken from Ref. [13].

A quadrant photodiode (QPD) is used to measure the confined particle's displacement fluctuations (Brownian motion). The QPD collects the detection laser's forward scattered light from the particle and produces a voltage output signal that is proportional to the particles displacement relative to the center of the trap (focus). A data acquisition card (DAQ) (NI-6221) collects the voltage signal, which is then captured by a custom LabVIEW program

(Mark Kendrick). A custom Mathematica program (Dr. David McIntyre) is used to obtain the trap stiffness and a MATLAB program is further used to analyze multiple data collection sets if necessary. An active picture of the experimental setup is shown in Appendix A.1.

3.2 Sample Cell Preparation

For trap stiffness experiments there are two types of microspheres normally used. Polystyrene (PS) microspheres of diameter $d = 0.99\mu m \pm 0.02\mu m$ (Duke Scientific) and silica (Thermo Scientific 8100 series) of diameter $d = 0.99\mu m \pm 0.02\mu m$. Particles are dispersed separately in deionized-water (Di-H_2O) (ϵ=80 @20°C) 10% by weight.

The mixture is inserted into a custom-made sample cell shown schematically in Figure 3.2a. The sample cell is prepared by placing a double-sided adhesive Secure-seal spacer (thickness $\approx 120\mu$m cut-out diameter = 20mm) on a clean glass microsphere slide (thickness $\approx 100\mu$m). Approximately 37μL of the mixture is placed within the circular cut-out spacer cell and a clean glass microscope cover-slip (22x22mm) is placed over the spacer cell sealing the mixture within the sample cell chamber.

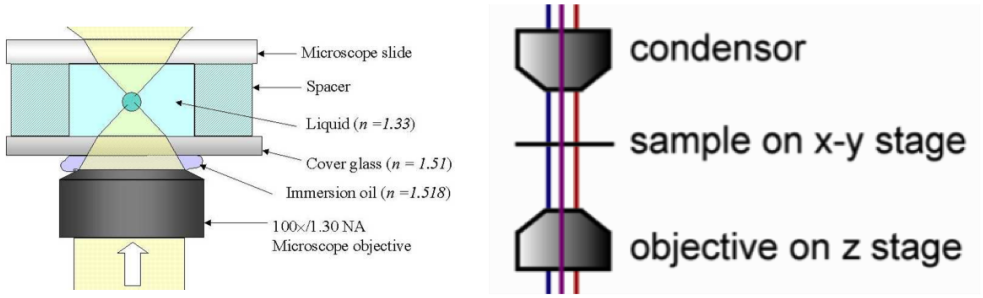

(a) Sample slide **(b)** Sample Position

Figure 3.2: (a) Depiction of a sample slide consisting of a glass cover-slip, adhesive spacer, and a glass sample slide, taken from Ref. [19]. The solution is placed within the spacer, between the sample slide and cover-slip. (b) Sample orientation within the optical trap. The sample is placed on a sample holder that places the sample between the objective and condenser with the cover-slip facing the objective.

The sample is then placed on a sample holder of the setup within the xy-plane, which is located between the objective and condenser (Figure 3.2b). The sample is positioned such that the cover-slip is facing the objective, and the immersion oil (type HF) is placed on the points of contact between the sample cover-slip and objective lens.

The use of immersion oil in optical trapping serves multiple purposes: (1) it is desirable to use an immersion oil that matches the index of refraction of the glass cover-slip. This property helps to minimize the loss of light, and thus trapping power when laser light passes transmits through the glass, (2) usually, immersion oil exhibits low fluorescence allowing the laser light to pass through with relatively low absorption, and (3) aids in protecting against optical damage, such as scratches, to the objective lens.

Chapter 4

Transverse Forces, Measurements, and Analysis

This section describes the forces on an optically trapped particle and the techniques used to model and calculate the optical trap strength, i.e spring constant k. Topics include the forces acting on a trapped particle, Brownian motion contributions, the mass-spring model, and the computational methods used to analyze a trapped microsphere.

4.1 Thermal Fluctuations of a Free Particle

In order to understand the forces on a trapped particle we first must discuss its motion in the absence of a trapping laser. A particle suspended in liquid undergoes random position fluctuations known as Brownian motion [20]. In short, Brownian motion arises from random forces due to thermal fluctuations of the surrounding medium, which can be envisioned as constant bombardment of molecules striking the particle surface. The theory of Brownian motion will not be discussed in this thesis, for further understanding on this topic see [20, 21, 22].

In one-dimensional space $\hat{x}$, the forces on a particle undergoing Brownian

motion are described through Newton's second law;

$$\sum_i F_i = m\frac{d^2x}{dt^2} = F_B(t) - \beta\frac{dx}{dt}$$

$$\Rightarrow \quad F_B(t) = m\frac{d^2x}{dt^2} + \beta\frac{dx}{dt} \tag{4.1}$$

where $\beta = 6\pi\eta a$ is the Stokes' drag coefficient for a submerged particle of mass m and radius a in a liquid of viscosity η, and $F_B(t)$ is the fluctuating force due to Brownian motion. Eqn 4.1 is known as the *Langevin Equation* [23] of a free particle in a liquid [21]. It is important to note that $F_B(t)$ is random, and therefore its average[1] value is zero $\langle F_B(t)\rangle = 0$, further details regarding this property will be discussed in Section 4.3.

4.2 Force Model of a Trapped Particle

In the presence of an optical trap the Brownian motion of a particle is suppressed, confining the particle to a region near the trapping laser focus. For small positional fluctuations within this region, coupled forces between the trapping laser and particle are (to a good approximation) **linearly proportional to the displacement** from equilibrium (laser focus). Therefore, the trapping laser applies a linear *restoring force* F_{trap} in 3-dimensions. This restoring force is comparable to a spring constant k in a mass-spring system, which is governed by Hooke's law $F = -kx$. Thus, the only adaptation to the current model Eqn. (4.1) is inclusion of this restoring force;

$$F_B(t) = m\frac{d^2x}{dt^2} + \beta\frac{dx}{dt} + k_{trap}x(t) \tag{4.2}$$

where k_{trap} denotes the trapping spring constant. The Langevin equation presented Eqn. (4.2) is known as the Brownian motion of a simple harmonic oscillator [21]

[1] The mean value (or average) will be denoted with angle brackets $\langle\rangle$.

Typically, when modeling the motion of sub-micron particles in a viscous fluid the Reynolds numbers are low ($R_e < 1$), which implies that $m\ddot{x} \ll (\beta\dot{x} + kx)$. This condition suggest neglecting the inertial (acceleration) term in Eqn. (4.2) resulting in

$$F_B(t) = \beta\frac{dx}{dt} + k_{trap}x. \tag{4.3}$$

This model[2] describing a thermally driven particle motion is commonly used in optical trapping analysis. As one may notice, Eqn. (4.2) is only dependent on three forces, the **restoring force** k_{trap}, the **drag force** $\beta\frac{dx}{dt}$, and the Brownian, or rather **thermal forces** $F_B(t)$ that are driving the harmonic oscillator. A cartoon depiction of these forces and how they relate to a mass-spring system is shown in Figure 4.1.

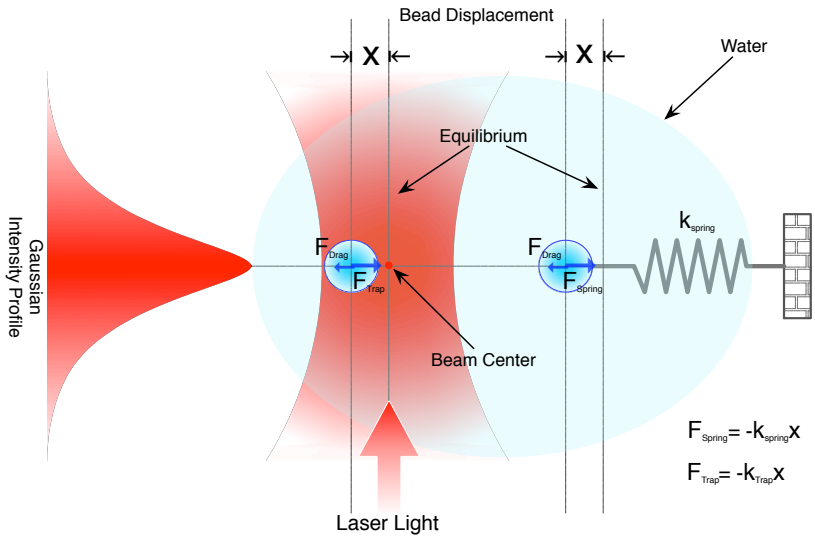

Figure 4.1: Depiction of the relation between a mass-spring system and a trapped dielectric sphere in 1-dimension $\hat{x}$.

[2]Note that gravitational effects have been neglected in this model.

4.3 Analysis of Trapping Force: Spring Constant k_{trap}

There are two independent methods used to determine the trapping force (spring constant) k_{trap} by acquiring the Brownian motion of a trapped particle. Employing multiple methods is particularly useful in cross-examining spring constant values, which provide key details involving the accuracy and reliability of the trapping apparatus.

The first method is through the equipartition theorem, from which the spring constant can be determined by the positional variance of a trapped particle's Brownian motion. Techniques also includes applying the equipartition theorem to a Gaussian fit of the position histogram and a quadratic fit to a reconstructed optical potential well. This method is useful for determining the trapping spring constant because the analysis is independent of the particle's radius a and surrounding viscosity η.

The second method, and usually considered the most reliable [24], is through a one-sided power spectrum analysis of the particle's position. The trapping spring constant is determined by fitting a Lorentzian and relating the corner frequency. Unlike the equipartition method, the power spectrum analysis relies on the particle's physical properties as well as its surrounding medium.

4.3.1 Method 1: Equipartition Theorem Analysis

Positional Variance

The equipartition theorem states that at a temperature T the average energy of any quadratic degree of freedom is $k_B T/2$. This theorem applies to *all* forms of energy (i.e. translational, rotational, vibrational, and elastic energy) for which the formula is a quadratic function of a dependent coordinate. This condition is met by our elastic potential energy model for the

spring constant

$$E(x) = -\int F_{trap} dx = \frac{1}{2} k_x x^2$$

yielding a harmonic potential (up to an integration constant). By relating positional variance and the equipartition theorem this becomes;

$$\frac{1}{2} k_x \sigma_x^2 = \frac{1}{2} k_B T$$

$$\Rightarrow \quad k_x = \frac{k_B T}{\sigma_x^2} \tag{4.4}$$

where k_B is Boltzmann's constant. Thus, by measuring a particle's Brownian motion and computing the positional variance the trapping spring constant is readily determined through Eqn. (4.4). Figure 4.2 displays the typical positional variance of a $1\mu m$ trapped polystyrene sphere.

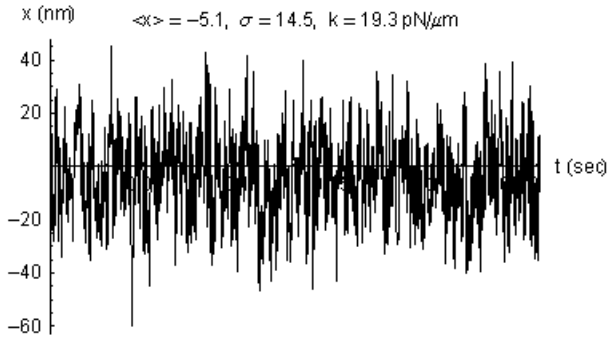

Figure 4.2: Positional variance of a trapped $1\mu m$ diameter transparent polystyrene sphere. Data collection perform with trapping laser power $\approx 37mW$ at a depth of $\approx 16\mu m$ from the sample cover slip (date: August 4, 2012).

Position Histogram

The spatial probability *density* function of a trapped particle over time can be described by Boltzmann statistics [25];

$$p(x)dx = Ce^{-\frac{E(x)}{k_B T}}. \tag{4.5}$$

The quantity $p(x)dx$ interpreted as the infinitesimal probability of finding a

particle at a position x over a infinitesimal space dx [26] in a potential $E(x)$, and C is a normalization constant. Since the energy for a harmonic potential is $E(x) = k_x\sigma_x^2/2$, Boltzmann statistics (Eqn. (4.5)) imply;

$$p(x)dx = Ce^{-\frac{E(x)}{k_BT}} = Ce^{-\frac{k_x\sigma_x^2}{2k_BT}}$$

$$\Rightarrow \quad k_H = \frac{k_BT}{\sigma_x^2}, \tag{4.6}$$

which is precisely the outcome (Eqn. (4.4)) of the previous *positional variance* technique.

This *positional histogram* technique may seem counterproductive and rather pointless based on the fact that the outcome Eqn. (4.6) is determined by implementing the equipartition theorem as was done in Eqn. (4.4). However, by fitting the histogram with a Gaussian curve and extracting the fitting parameters (constants) the spring constant k_H can be determined. **Note** that the spring constant is labeled with the subscript H, meaning the $\hat{x}$ directional spring constant deduced by the position histogram technique[3]. Figure 4.3 displays the positional histogram (red bins) and Gaussian fit (black curve) of the Brownian particle from Figure 4.2.

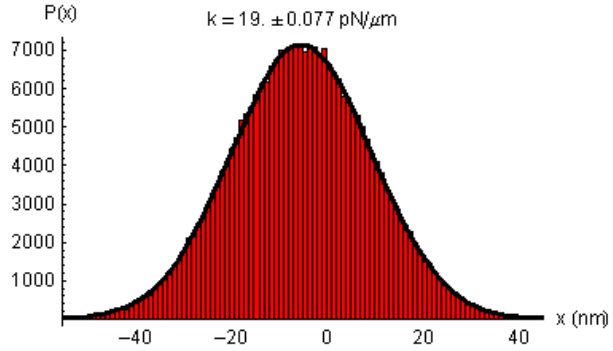

Figure 4.3: Typical position histogram and Gaussian fit of a trapped $1\mu m$ diameter transparent polystyrene sphere. Data collection perform with trapping laser power $\approx 37mW$ at a depth of $\approx 16\mu m$ from the sample cover slip (date: August 4, 2012).

[3]The position histogram technique is a form of *data compression* called *windowing*, see Ref. [27] for more information involving data compression and optical tweezers.

The height of each histogram bar $p(x)$ corresponds to the number of occurrences the particle was detected at a particular distance from the center of the optical trap. The *spread* (width) of the Gaussian distribution curve is proportional to the trapping spring constant k_H, assuming room temperature $T = 298K$. Thus, by fitting the histogram with a Gaussian distribution the k_H can be determined.

Potential Well

The final technique used to obtain the trapping spring constant is by reconstruction of the potential well from the position histogram and fitting a parabola. According to Florin [25] the potential $E(x)$ experienced by the particle is found by taking the logarithmic of Eqn. (4.5);

$$E(x) = -k_B T ln(p(x)) + k_B T ln(C), \tag{4.7}$$

where the term $k_B T ln(C)$ is the well offset (average value, which in theory is zero) and will be neglected.

Next, consider the potential energy of a particle in a harmonic potential well modeled by a mass-spring system, which is proportional to the squared displacement;

$$U = -\int F_s(x)\, dx = \frac{1}{2} k_{trap} x(t)^2$$

$$\frac{1}{2} k_{trap} x(t)^2 = a x(t)^2 \tag{4.8}$$

Eqn. (4.8) states that it is possible to extract the spring constant by fitting a parabola and extracting the fitting parameters. This expression is related to the analytical solution of Eqn. (4.7),

$$E(x) = \frac{1}{2} k_{trap} x(t)^2 = -k_B T ln(p(x))$$

$$\Rightarrow \quad k_w = \frac{-2 k_B T}{x\,(t)^2} ln(p(x)). \tag{4.9}$$

For this reason the spring constant, denoted as k_w, is obtained by fitting a parabola to the logarithmic values of the positional histogram and extracting the fitting parameters.

Figure 4.4 displays the potential well of the histogram occurrences (dots), which is fitted to a parabola (black line). Notice that the histogram data (dots) near the ends of the plot tends to have a larger spread from the fit. This is due to the small sample size at large distances from the trapping center. Meaning that the trapping forces cause the particle to spend more time in the middle (i.e. lower potential energies) rather than at large distances from the laser focus.

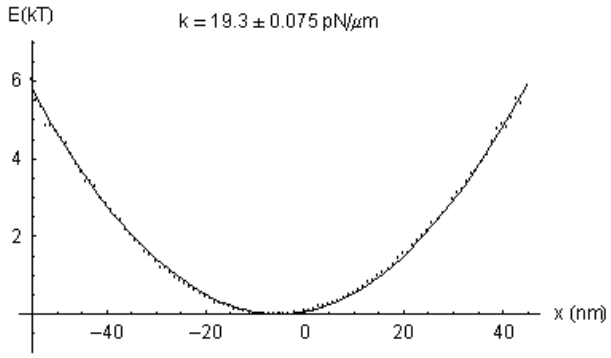

Figure 4.4: Typical potential well and fit of a trapped $1\mu m$ diameter transparent polystyrene sphere. Data collection perform with trapping laser power $\approx 37mW$ at a depth of $\approx 16\mu m$ from the sample cover slip (date: August 4, 2012).

4.3.2 Method 2: Power Spectrum Analysis

The power spectral density (power spectrum or PSD) of a trapped particle is a method used to analyze its motion signal in the *frequency* domain $x(f)$, as opposed to the *time* domain $x(t)$ in Figure 4.2. This analysis method is considered the most reliable [24] and is particularly useful in cross-referencing with the equipartition techniques outlined in Section 4.3.1 because it takes into consideration the physical properties of the trapped specimen and its surrounding liquid. Mapping to the frequency domain is achieved by taking the Fourier transform of the Brownian motion $F_B(t)$ with respect to time of

the particle's trajectory $x(t)$ represented in Figure 4.2. The central purpose of this transformation is that the frequency response of the particle's motion reveals an attribute that is related to the trap stiffness.

Brownian motion is presented theoretically as the Langevin equation illustrated in Eqn (4.3), which is once again;

$$F_B(t) = \beta \frac{dx}{dt} + k_{trap} x. \tag{4.10}$$

The solution to this equation can be found by taking the Fourier transform,

$$F_B(t) = \beta \frac{dx}{dt} + k_{trap} x \quad \xrightarrow{\mathcal{F}} \quad \tilde{F}_B(f) = (i\beta 2\pi f + k_{trap})\tilde{x}(f). \tag{4.11}$$

and taking the square of the complex norm;

$$|\tilde{F}(f)|^2 = (\beta^2 4\pi^2 f^2 + k^2)|\tilde{x}(f)|^2. \tag{4.12}$$

$|\tilde{F}(f)|^2$ holds physical value of the energy content per unit frequency interval, namely *power spectrum*. Whereas, the power spectrum $|F(t)|^2$ is proportional to the total energy of the oscillatory system. Accordingly, both $|\tilde{F}(f)|^2$ and $|F(t)|^2$ are interprets of energy [28].

As mentioned in Section 4.1 the thermal fluctuations of a trapped particle is considered random with zero mean $\langle F_B(t) \rangle = 0$. R. Kubo describes in a report on the classical Langevin equation [29]; under the assumptions that $F_B(t)$ is (1) a Gaussian process, and (2) its correlation time is infinitely short, the power spectrum of $F_B(t)$ is equal to a constant. These characteristics imply that the random Brownian force $F_B(t)$ has a *white spectrum* and is considered white noise[4]. Thus, the constant[5] denoting the one-sided thermal power spectral density per unit time is [30, 21];

$$G_o = |\tilde{F}(f)|^2 = 4\beta k_B T. \tag{4.13}$$

[4]White noise is a random signal with a flat (constant) power spectral density.
[5]For the relation of Eqn. (4.13) and further explanation see Appendix A.2.1.

Relating Eqn. (4.12) and (4.13) gives,

$$4\beta k_B T = (\beta^2 4\pi^2 f^2 + k^2)|\tilde{x}(f)|^2$$

$$|\tilde{x}(f)|^2 = S_{xx}(f) = \frac{k_B T}{\pi^2 \beta \left(f_c^2 + f^2\right)}. \tag{4.14}$$

For a particle in a harmonic potential, $S_{xx}(f)$ corresponds to the expected one-sided power spectral density per unit time, which is that of a Lorentzian curve with corner frequency f_c that is proportional to the trap strength $f_c = k_{trap}/2\pi\beta$. Therefore, by expressing a trapped particle's position $x(t)$ in terms of frequency components a Lorentzian fit to the power spectrum $S_{xx}(f)$ will yield the trap spring constant k_s [31, 12, 30].

Figure 4.5 displays the power spectrum of a trapped $1\mu m$ polystyrene sphere corresponding to the trajectory $x(t)$ shown in Figure 4.2. From the Lorentzian fit (black line) of the windowed data (dots) the corner frequency can be easily determined.

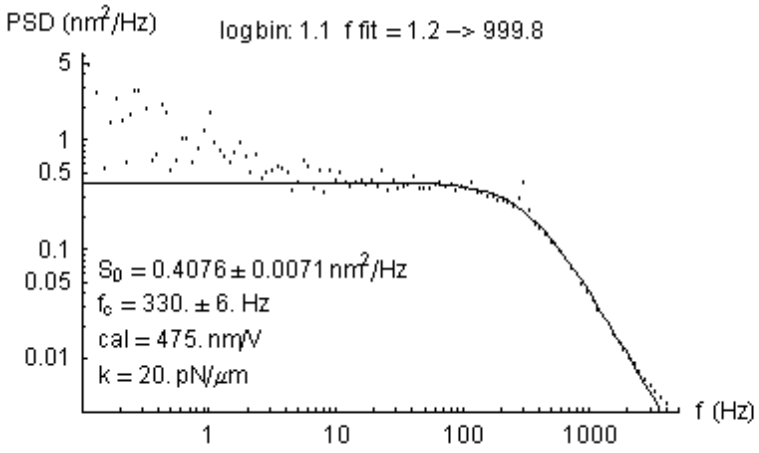

Figure 4.5: Typical power spectrum (dots) and Lorentzian fit (solid line) of a trapped $1\mu m$ diameter transparent polystyrene sphere. Data collection perform with trapping laser power $\approx 37mW$ at a depth of $\approx 16\mu m$ from the sample cover slip (date: August 4, 2012).

For details pertaining to the methods included in this section see [27, 32].

Chapter 5

Force Measurement Calibrations

Techniques described in this section are designed to calibrate the quadrant photodiode (QPD) detection signal in order to accurately track a trapped particle's movement. As Neuman and Block state in their 2004 overview of optical trapping [12], "accurate position calibration lies at the heart of quantitative optical trapping." There are several position calibration methods, which are dependent upon the chosen position detection scheme and the ability to move the trap and/or sample holder stage [12].

The main ideas behind the calibration procedure is to ensure proper coalignment (overlap) between the trapping and detection laser at the trapping plane and centering the back focal plane image onto the QPD detection sensor. Detection laser calibrations consists of two calibration methods, one preformed by imagining a particle attached to the cover-slip, and then imagining a trapped particle at the intended trapping depth from the surface of the microscope cover-slip. Depth calibration presented in the following sections are all preformed at $\approx 16\mu m$ from the cover-slip surface, into the sample.

5.1 Optical Tweezer Calibrations

The sample-slide is placed on an adjustable xy-plane sample holder. The holder positions the sample-slide within the trapping plane of the inverted microscope, which lies between the objective and the condenser. An encoder-mike controller (Oriel 18011) is used to move the objective in the axial-direction ($\hat{z}$). This therefore moves the trapping plane towards the cover-slip and into the sample. The images produced by the inverted microscope are projected into a CCD (charged-coupled device) camera and viewed on a monitor shown in Figure 5.1. By moving the trapping plane into the sample

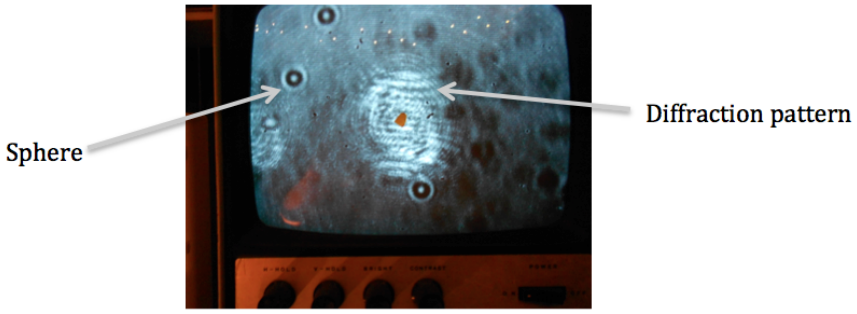

Figure 5.1: Picture taken of the viewing monitor from a depth of 16μm within a sample of polystyrene spheres. The white circular rings are diffraction fringes produced by the detection laser. Three microspheres are shown.

we are able to identify when the trapping laser focal point passes the cover-slip and enters into the sample by viewing the diffraction pattern on the CCD camera. At this point the objective is stopped and a sphere attached to the cover-slip is found by manually moving the sample holder. Attached spheres are those that do not undergo random Brownian motion and are physically stuck to the cover-slip. Differentiating the two is quite simple. Stuck spheres do not move.

5.1.1 Cover-slip Calibrations: Immobilized Particle

Cover-slip calibration is achieved by inducing particle movement and mapping the displacement of the sphere relative to the focus. The sample holder is oscillated with a piezo-electric material, which changes lengths when a electric potential is applied. By oscillating the stage with a sinusoidal potential while mapping the particles displacement with the detection laser we are able to analyze its displacement in terms of output voltage from the QPD. We expect the restoring force to be linear through the equilibrium position of the trap, which coincides with the mass-spring model. In addition, the particle position should be symmetric about the equilibrium point because the stage is being driven by a symmetric (AC) electric-field.

Figure 5.2 displays the oscilloscope response of an attached bead to the cover-slip when the piezo-electric stage is driven by a continuous 300mV sinusoidal waveform. The voltage response is produced by a quadrant photodiode (QPD) detector, which produces voltage response proportional to the bead's displacement through the detection laser. Calibrations and measurements are usually performed using a QPD gain setting of 100.

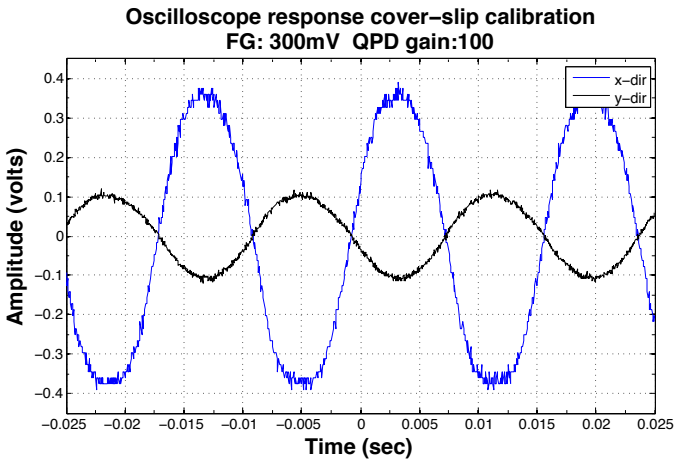

Figure 5.2: Oscilloscope response of an immobilized sphere in continuous mode. Function generator settings: 300mV$_{pp}$ frequency: 61Hz QPD gain: 100

Figure 5.2 display typical QPD responses for the specified function gen-

erator settings. As mentioned, the key features of these calibrations is to gain a symmetric response about the zero axis, and linear response through the axis. Both quantities correspond to the alignment and projection of the detection laser into the QPD. In addition, these procedures also gain insight into how well the trapping laser is aligned through the objective-condenser pair.

5.1.2 Depth Calibration: Brownian Motion

The second procedure in the calibration process is analyzing the displacement of a trapped sphere at a known depth within the sample. For reliable and reproducible results, I have chosen to use a depth of 16μm for all of my depth calibration. I chose this depth because trap strength measurements will be conducted at this depth, for that reason a calibration at the same depth is logical in producing the best possible consistent results. This calibration resembles the cover-slip calibration process, in that, calibrations are performed first with a continuous wave (cw) potential mode, and then a 2-cycle burst mode.

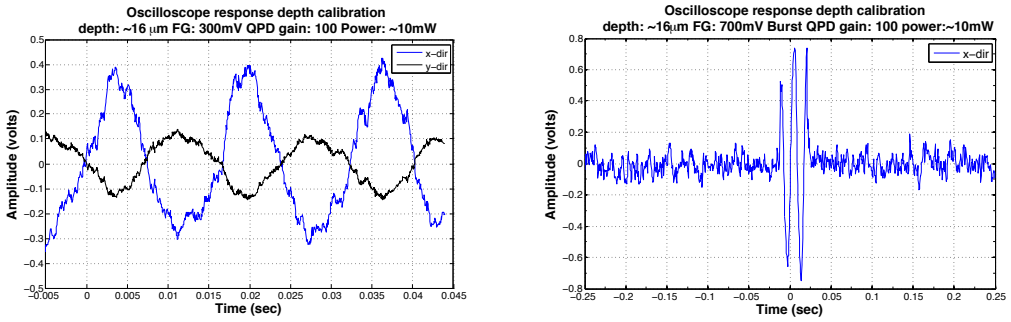

(a) depth calibration CW **(b)** depth calibration burst

Figure 5.3: Depth calibration oscilloscope response for a trapped sphere in continuous and burst mode

Methods using the cw mode is comparable to those used in the cover-slip calibration. A sphere is trapped using at 10mW and the displacement signal is viewed on the oscilloscope (Figure 5.3a). The signal produced by the

oscilloscope is expected to resemble an amplitude response comparable to the cover-slip calibration (Figure 5.2), except for a slightly minimized amplitude response cause by the trapping laser forces.

The main goal of this calibration procedure is to ensure the detection laser is properly overlapping the trapping laser at the intended trapping depth. At this point it is easy to see whether or not the overlapping of the trapping and detection laser is reasonable. Slight "tweaking" of L3, which controls the path of the detection laser, may be needed to produce a symmetric oscilloscope response. The 2-cycle burst mode calibration (Figure 5.3b) is one of the best indication of the overlapping. This mode allows observation of the Brownian motion response after the bust. It has been observed that for optimal trap stiffness measurements the"tailing" noise (Brownian motion) exhibits rapid decay after the bust that leads into symmetric noise, as seen in Figure 5.3b.

Chapter 6

Trap Strength Experiments

Experiments performed in this chapter are designed to measure the trapping force on colloidal microspheres suspended in water. Numerous experiments were organize to investigate the reproducibility and accuracy of the measured trapping spring constant[1] k and calibration factor $1/\rho$ (Eqn. (6.1)). Experiments and their results in this chapter include: Chapter 6.2 power dependence, Chapter 6.3 sphere-to-sphere variation, and Chapter 6.4 depth dependence.

6.1 Determining Trap Stiffness: An Example

Trap stiffness k and calibration $1/\rho$ quantities are obtained by acquiring the transverse $\hat{x}$ time series displacement of a trapped particle undergoing Brownian motion (Figure 6.1a). These experiments are essentially testing how well the trapping laser is aligned through the inverted microscope while simultaneously testing the coalignment of the detection laser to the trapping laser, as well as the detection subsystem accuracy. Details regarding these characteristics will be further examined in each result discussion section proceeding the experiment.

[1]The terms *spring constant*, *trap strength*, and *trap stiffness* are equivalent in meaning and are used interchangeably throughout.

All experimental spring constant values are determined by analyzing the LabVIEW signal response through a custom Mathematica program. This program applies the analysis methods outlined in Section 4.3 with slight experimental adjustments that involve a calibration factor ρ.

The calibration factor is, as it sounds, a constant value that calibrates the QPD *voltage* signal into usable values of *displacement*, namely nanometers. This is achieved by adjusting the PSD in Eqn (4.14) to the QPD signal by adding a linear *calibartion* constant denoted[2] as ρ, which holds units of voltage per unit of displacement $[V/nm]$.

For example, the spring constant k_x of a $1\mu m$ polystyrene sphere having a measured displacement variance from equilibrium σ_x^2=$(14.5nm)^2$ (Figure 6.1a) is first acquired through the equipartition theorem (Eqn. (4.4));

$$\frac{1}{2}k_BT = \frac{1}{2}k_x\sigma_x^2 \Longrightarrow k_x = \frac{k_BT}{\sigma_x^2},$$

yielding a value of k_x=19.36 $pN/\mu m$.

[2]Note that the calibartion factor corresponding to *cal* within the Mathematica computations is equivalent to the inverse of ρ, $cal = 1/\rho$

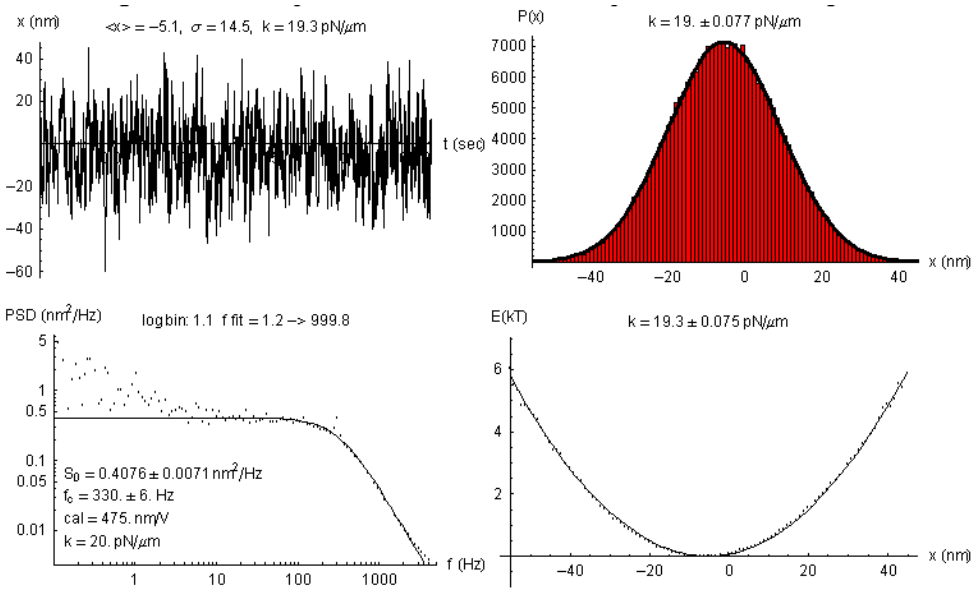

Figure 6.1: Mathematica data analysis of the suppressed Brownian motion of a $1\mu m$ polystyrene sphere at a sample depth of $\approx 16\mu m$ and trapping laser power $37mW$ at $795nm$ wavelength. a) Time series of the suppressed Brownian motion from which k_x is computed through the equipartition theorem. b) Histogram (bin) of the particle's displacement from the mean, from which k_H is computed through extracting fit parameters. c) Power spectral density (PSD) from which k_s is computed by obtaining the corner frequency. d) Potential well analysis of the histogram from which k_w is computed through fitting parameters.

The k_s spring constant is next obtained by analyzing the calibrated power spectrum of the particle's position fluctuations, which is related to the Fourier transform of Figure 6.1a;

$$S_{vv}(f) = \rho^2 \frac{k_B T}{\pi^2 \beta \left(f_0^2 + f^2\right)}. \tag{6.1}$$

where β=$6\pi\eta a$ is defined as the viscus drag coefficient (Stokes) in water, f is the frequency (Hz), and f_c=$k_s/2\pi\beta$ is the corner frequency. The results shown in Figure 6.1c yields a corner frequency of f_c=330 Hz with a displacement-to-voltage calibration factor of $1/\rho$=475 nm/V. Thus, by relating the corner frequency and spring constant we obtain k_s=19.5 pN/μm.

The trap stiffness is also obtained by fitting a Gaussian (normal distribu-

tion) curve to the positional histogram in Figure 6.1b. A byproduct of this method is the optical potential well, which is essentially fitting the histogram distribution in units of energy, i.e. logarithmic scale Figure 6.1d.

$$p(x) \propto exp\left(-\frac{U}{k_B T}\right) = exp\left(\frac{k_h x^2}{2k_B T}\right). \tag{6.2}$$

The fitting parameters are then extracted yielding a trap strength for the histogram fit of k_H=19.2 $pN/\mu m$, and k_w=19.3 $pN/\mu m$ for the potential well fit. The required specification for a reliable and accurate trap is that all four methods yield a spring constant to within 10%.

6.2 Power Dependence Measurements

Experiments involving power dependence measurements were performed on 1μm (σ=0.02μm) diameter transparent polystyrene (Duke Scientific) and 0.99μm (σ=0.02) silica (Thermo Scientific) microspheres suspended deionized water. Sample cells were prepared by the techniques outlined in Chapter 3.2. Measurements were taken with a trapping wavelength near 800nm and optical powers ranging from 10mW to 37mW (as measured before DM2 Figure 3.1) at a trapping-plane depth of ≈16μm from the sample cell cover slip.

Figure 6.2 displays the measured spring constant k_x over a span of optical powers ranging from 10-30mW. Each power dependence measurement was conducted on the same microsphere as a control to eliminate uncertainties involving sphere-to-sphere diameter deviations.

The plotted points in Figure 6.2 correspond to the average measured spring constant computed via Mathematica. Each data collection set contains four 30 second data runs, yielding four values for the spring constant within a standard two minute testing time. The k_x, k_h, k_s, k_w, and calibration factor $1/\rho$ values are imported into a custom MATLAB program. The MATLAB program averages each spring constant method value over each

30 second run, computes the standard deviation, fits a linear regression to the average values for the range of optical powers, and plots the spring constants and calibration factors with error bars corresponding to the standard deviation from the mean.

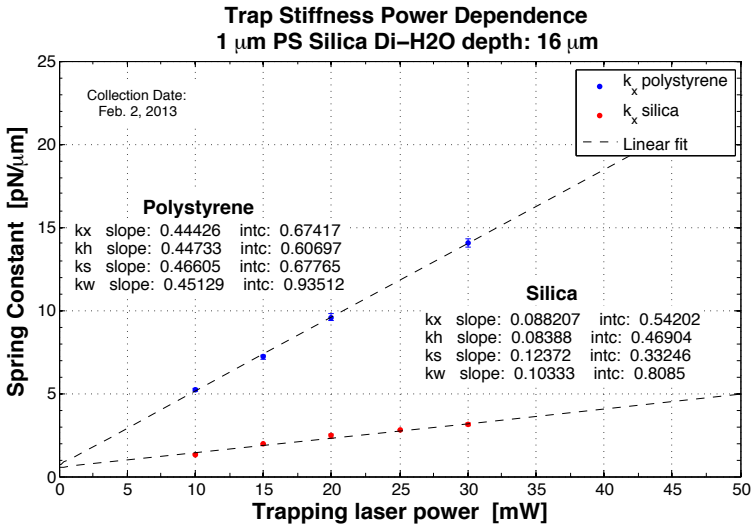

Figure 6.2: Trap strength power variance measurements for polystyrene and silica microspheres suspended in deionized water. Inset: Linear fit parameters obtained from the Mathematica trap stiffness methods k_x, k_h, k_s, k_w.

For example, a four data run set corresponding to an optical power of $10mW$ is circled in Figure 6.2. This particular dataset produced spring constants $k_x = 5.34, 5.28, 5.12,$ and 5.14 $(pN/\mu m)$. The MATLAB program computes and plots the mean value $k_{mean} = 5.22$ $(pN/\mu m)$ and standard deviation $k_{SDiv} = 0.11$ $(pN/\mu m)$. Similarly, the calibration factors are averaged and plotted in the same manner Figure 6.3.

Figure 6.3 displays the displacement-to-voltage calibration factor $1/\rho$ corresponding to Figure 6.2 for each optical trapping power. The calibration factor is the value needed to convert the QPD voltage signal to displacement (nm), which is used within the Mathematica computations to resolve each spring constant value via power spectrum. The calibration factors are first approximated in the initial trap stiffness computation and later re-iterated with a more accurate value.

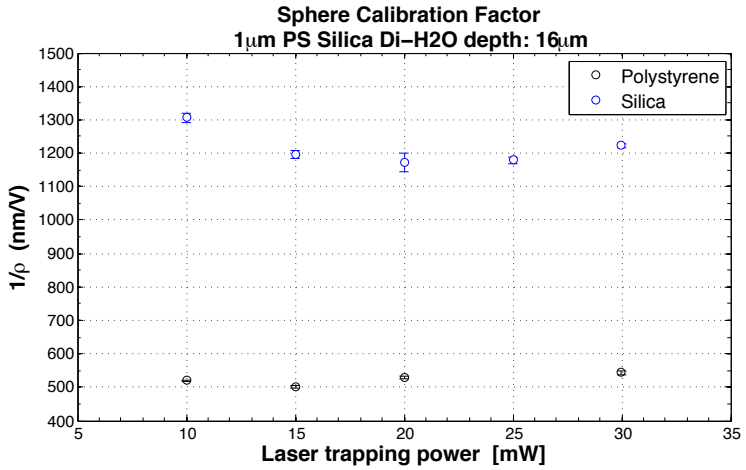

Figure 6.3: Averages of the displacement-to-voltage calibration factors used in the Mathematica computations to resolve the trap stiffness.

To ensure reproducibility, power dependence measurements were performed on multiple samples over an extended time period between experiments. Figure 6.4 displays trap stiffness measurements conducted during different trial days for polystyrene spheres. Each experiment was performed under the condition of total realignment and calibration of the apparatus.

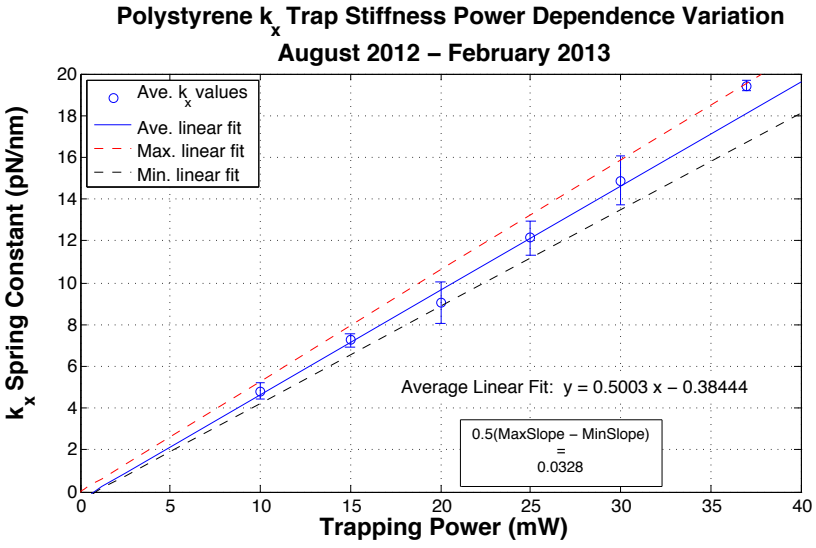

Figure 6.4: Polystyrene power reproducibility.

Figure 6.4 displays power reproducibility values of all polystyrene power dependence experiments (circles) between August 2012 to February 2013. Error bars are the standard deviation from the mean, which is fitted to a linear best fit (solid line) using the least squares method. (Dashed lines) the maximum and minimum slopes within the limits of the error bars. **Note:** Measurements at power 37mW is not included in the fitting due to limited data.

Discussion

The trap strength spring constants presented in Figure 6.2 exhibit a linear dependence with optical trapping powers. This response is expected from the assumptions and analysis outlined in Section 4, in the view of the fact that trap stiffness is determined by modeling the trapped particle as a mass-spring system. Thus, increasing the power of the trapping laser is analogous to attaching a stiffer spring to the system in Figure 4.1.

From Figure 6.2 it is easy to see a large differentiation between the trap stiffness of silica and polystyrene spheres. One important factor is that the Mathematica program used to compute the trapping spring constant is designed for polystyrene microspheres based on [27], which does not account for the relative index of refraction between the particle and its surroundings. This discrepancy is not too worrisome, in that, further experiments including silica spheres can be normalized to the trapping spring constants of polystyrene, which are well known. Work on this relation has been modeled and simulated in [13].

The calibration factor results shown in Figure 6.3 display a constant relation over the range of powers. This trend is expected because the calibration factor $1/\rho$ is the factor used in converting the QPD signal from a measure of electric potential (Volts) to displacement (nm), which should not change with increasing/decreasing powers. The main concern in calibration factor is large 'drifting' to either higher or lower values between experiments.

Figure 6.4 exhibits some rather interesting effects, in that, it shows how

the trap stiffness deviation from the mean starts to increase at higher powers, which can be seen from the maximum and minimum fit lines. This deviation is actually expected, because the expansion lens (L3 Figure 3.1) is positioned/calibrated for trapping near 10mW. As the powers increase the radiation pressure (incident photon force) increases, pushing the particle deeper into the sample. As a result, the detection laser focal plane isn't centered 'on' (or near) the center of the trapped particle, instead it is higher (or deeper into the sample). Thus, the diffraction-limited focal point of the detection laser has begun to spread out, which not only changes the geometry of the back-focal plane interferometer but it also begins to veer.

6.3 Sphere-to-Sphere Variation Measurements

Sphere-to-sphere variation measurements are performed in this section on $1\mu m$-diameter polystyrene beads at a trapping depth $\approx 16\mu m$ from the glass cover-slip. These experiments serve to provide an experimental estimate on the particle diameter uncertainties. The polystyrene spheres used in the following experiment are known to have $\pm 0.02\mu m$ diameter deviation.

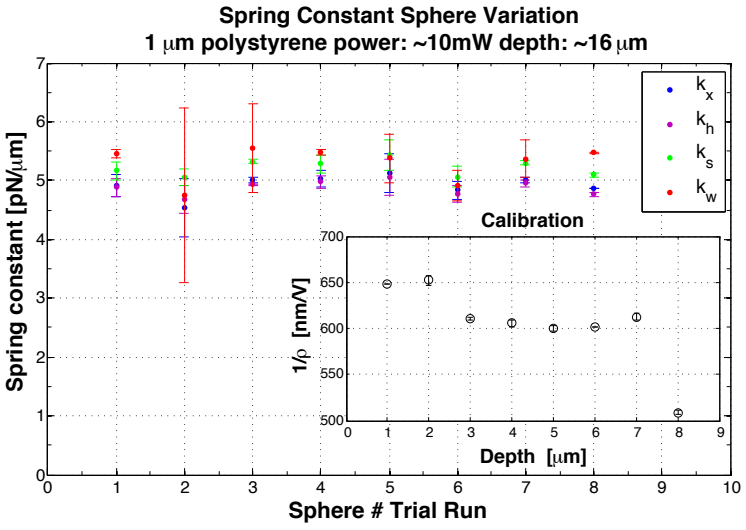

Figure 6.5: Polystyrene spring constant sphere and calibration factor (inset) variance.

Discussion

Figure 6.5 displays spring constant results for eight different polystyrene microspheres in water. The plot displays spring constant values k_x, k_h, k_s, k_w corresponding to the Mathematica calculation methods described in section 4.3. The error bars correspond to the standard deviation between the number of data runs acquired during each trial. In this particular experiment there were only two data runs per trial dataset. Because of the low number of data runs the standard deviation is only a comparison between two values. For more accurate results, increased data runs are needed.

6.4 Depth Dependence Measurements

Trapping spring constant k_x depth dependence for $1\mu m$ polystyrene sphere were also explored. Depth dependence measurements insure proper depth to eliminate thermal contribution from the glass cover-slip. It is expected to see large trap strength variations near the cover-slip and at large depths, due to the limiting numerical aperture of the oil immersed objective. Measurements were performed on the same sphere over a range of $2\mu m$-$22\mu m$, results for k_x are shown in Figure 6.6.

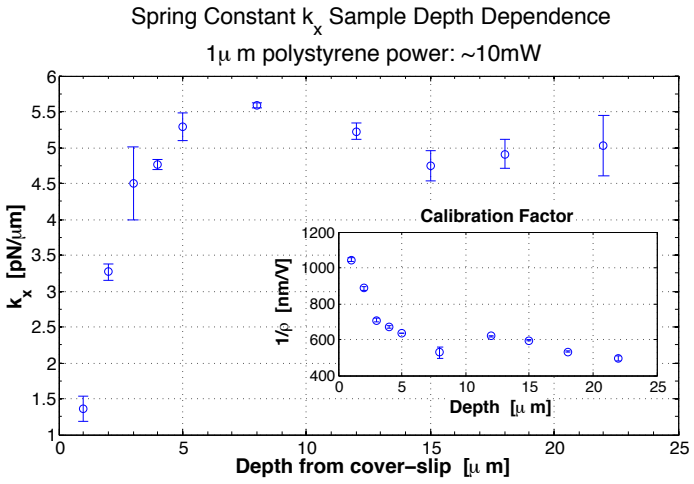

Figure 6.6: Trap spring constant k_x and calibration factor (inset) sample depth dependence, with standard deviation error bars.

Discussion

As expected, near the cover-slip, there are large thermal contributions coupled with the trapping forces, resulting in a lower trapping spring constant. It is important to note that this type of experiment is much trickier than it seems because it's extremely difficult to *exactly* co-align the detection and trapping lasers during the alignment procedure. In consequence, as the trapping plane goes to increased depths into the sample the detection laser tends to veer. To compensate, at each depth measurement presented in Figure 6.6 a quick calibration was performed to roughly overlap both lasers.

6.5 Conclusion

From the discussion and results presented in section 6.2, it has been shown that the optical tweezer apparatus exhibits, as expected, linear power dependence for polystyrene and silica trap stiffness constant k_{trap}. We can conclude from this that our procedures provide reproducible trap stiffness value to within an experimental uncertainty of 10.5% for $1\mu m$ polystyrene microspheres at trapping powers near 15mW. This confirms that these procedures can provide accurate trapping measurements in the transverse $\hat{x}$ direction near trapping powers of 15mW. However, large variations in spring constant values have been observed at increasing powers due to underlying effects. These effects have been hypothesized to be caused by increase radiation pressure at powers $> 20mW$.

In addition, the findings presented in sections 6.3 show the expected constant trend between multiple polystyrene microspheres. Similar results for $1\mu m$-diameter silica spheres have also been observed (not shown). Section 6.4 confirms that at small trapping depths ($< 4\mu m$) thermal fluctuations contribute greatly in measuring the trapping spring constant. At increased depths ($< 22\mu m$) constant trap stiffness values are obtained as expected. This confirms that at a trapping depth of $\approx 16\mu m$ there are minimal to no thermal contributions.

Chapter 7

Preliminary Surface Charge Measurements

This chapter presents preliminary studies involving optical tweezer-based surface charge measurements of colloidal silica microspheres dispersed in water. Techniques developed by [8] are implemented to establish methods necessary to preform, detect, and measure electrophoretic contribution. The electrophoresis experiment in this section is designed to measure the effective surface charge Z_{eff} response at relatively low (AC) electric-field frequencies near the optical trap corner frequency.

7.1 Basic Principles and Model

Surface charge measurements are most readily preformed through electrophoresis experiments, that is, measuring a particle's displacement in the presence of an (AC) electric-field perturbation. The electric-field introduces Coulomb-force interacts with charges near the particle surface creating an electrokinetic force, which induces particle movement. As the particle moves through the liquid, surrounding ions are continually binding to, and dissociating from, the particle surface yielding a fluctuating effective surface charge value. However, the amount by which the particle is displaced is related to the electric-field

perturbation amplitude E_{AC}.

With the electric-field perturbation addition there are now three forces acting on the optically trapped microsphere: (1) photonic restoring forces F_{trap}, (2) Stokes frictional forces F_{drag}, and (3) a harmonic electric-field force $F_{AC} = Asin(2\pi f_E t + \phi)$. The equation of motion is the superposition of these three forces, namely;

$$m\frac{d^2x}{dt^2} + \beta\frac{dx}{dt} + k_{trap}x(t) = Asin(2\pi f_E t + \phi) + F_B(t). \tag{7.1}$$

Where $F_B(t)$ represents the random thermal Brownian motion (Gaussian process), and defining the *effective*[1] electrokinetic surface charge $Z_{eff} = A/E_{AC}$, which is holds units of fundamental charge q_{el} [8].

The motion equation Eqn. (7.1) can be averaged together to get a correlations function $\mathcal{C}(t)$ which then can be expressed as a normalized function in terms of the parameter γ^2, a scaled ratio between the mean-square electric-field force and the Brownian thermal forces;

$$\gamma^2 = \frac{\langle F_E^2\rangle/\langle F_E^2\rangle}{1 + (\omega_E/\omega_c)^2} \tag{7.2}$$

where $\langle F_E^2\rangle = Z_{eff}^2 e^2 E^2/2$ and $\langle F_E^2\rangle = k_B T k_{trap}$. This scaling ratio γ is the most common value extracted in practice [8], and solving for the effective surface change Z_{eff} comes easily;

$$|Z_{eff}|q_{el} = \frac{\gamma\beta}{E}\sqrt{\frac{2k_BT}{k_{trap}}(\omega_E^2 + \omega_c^2)} \tag{7.3}$$

where $\beta = 6\pi\eta d$ Stokes' drag constant and $E = V/d$ is the amplitude of the applied (AC) electric-field measured in units of *volts per meters*. Taking the

[1] The effective value of an alternating quantity is merely the expected value, or root-mean-square.

Fourier transform of Eqn. (7.3) yields;

$$\Rightarrow \quad \tilde{x}(\omega) = \frac{k_B T}{\pi \beta} \frac{1}{(\omega^2 + \omega_c^2)} + \frac{k_B T \gamma^2}{2 k_{trap}} \Big[\delta(\omega - \omega_E) + \delta(\omega + \omega_E) \Big]. \tag{7.4}$$

Eqn. (7.4) describes the power spectral density function of the trapped particle within the presence of an applied (AC) electric-field[2]. Notice that the first term exhibits Lorentzian properties comparable to a Brownian particle in a harmonic potential well. As expected, this term is equivalent to the power spectral density of a trapped panicle, that is, Eqn. (4.14). However, the second term is a superposition of two delta functions, which arises from the (AC) electric-field perturbation, where $\omega_E = 2\pi f_E$ is the driving frequency. The delta functions are defined as being equal to one if $\omega_E = \omega$. Therefore, we would expect the PSD to contain a peak-value at the electric-field frequency that is proportional to γ^2, which can be found extracting the electric-field PSD contribution and integrating over all frequencies [8].

In short, by tracking a trapped particle within the presence of an external (AC) electric-field and expressing its motion in frequency components (PSD), a peak at the driving voltage frequency will occur. The peak value is proportional to the scale ratio γ^2, and thus, the effective surface charge Z_{eff} Eqn. (7.3) carried by the particle. An estimate for the effective surface charge can be calculated by finding the area under the peak value of the PSD.

Corollary

It is important to note that this method is only valid for small ion concentrations where the *zeta potential* (electrokinetic potential) at the hydrodynamic slipping plane boundary of the double layer is small. In which case the Huckel limit is valid and the electrophoretic mobility is proportional to the surface charge. Outside of this limiting case, increased ion concentrations form a

[2]Eqn. (7.4) describes the two-sided PSD, which is composed of real and imaginary parts, in practice the one-sided PSD is normally used, yielding only one delta function.

thickened cloud (double layer) around the particle, results in large screening effects. Upon particle movement, the thickened double layer is more susceptible to large deformation, in which case the relaxation effects perturb the electrophoretic mobility, consequently giving rise to disproportionality between the mobility and zeta potential.

7.2 Preliminary Surface Charge Experiments

Modified Sample Cell Preparation

Samples are prepared in a custom sample cell holder similar to the procedures outlined in section 3.2, with slight modifications. Modifications include fastened electrodes and the ability to reuse the sample cell. Electrophoresis sample cell are prepared dry by gluing two thin aluminum strips separated by about $100\mu m$ to a microscope cover-slip. A small slit is cut through the microscope slide using a DREMEL rotary diamond wheel (545), used to load/reload and wash out the sample cell.

An adhesive spacer is placed on the microscope slide and a small channel $\approx 1mm$ wide is cut out and removed to allow fluid flow while cleaning and reloading the cell. The electrode/cover-slip is placed on the spacer and the edges are glued to help prevent leakage through the spacer walls. Silica microspheres (Thermo Scientific 8100 series) of diameter $d = 0.99\mu m \pm 0.02\mu m$ dispersed in deionized-water (ϵ=80 @20°C) 10% by weight and is injected into the sample cell through the slit in the microscope slide.

7.2.1 Silica Frequency Dependence

Electrophoresis experiments were performed on silica particles with a laser trapping power of $10mW$, $790nm$ wavelength, at a trapping depth of $\approx 16\mu m$ from the cover-slip. The electrode separation was measured to be $\approx 106\mu m$ along the $\hat{x}$-direction of the sample. A trapped sphere was positioned at the midpoint between the electrodes and a (AC) electric-field was applied across

the electrode channel using a Tektronix function generator (AFG 3021). The electric-field strength was calculated under the assumption of ideal parallel-plate, $E = V/d$. A sinusoidal potential with zero DC offset $8.533V_{pp}$ was supplied to the electrode connections by the function generator, resulting in $E_{AC} \approx 40kV/m$. Figure 7.1 shows the electrode sample cell positioning within the optical tweezer apparatus.

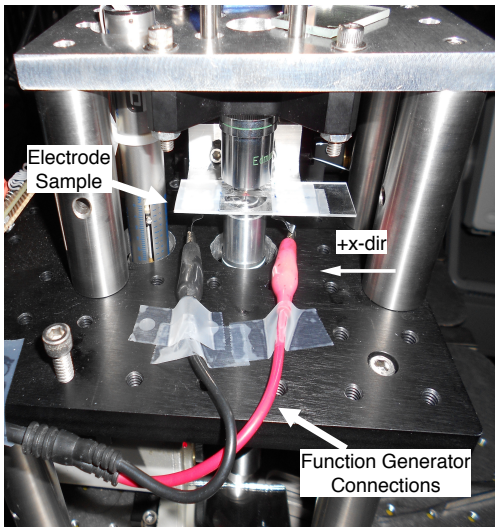

Figure 7.1: Electrode sample and position for electrophoresis experiments.

The particle displacement was acquired by a quadrant photodiode and trapping spring constant measurements were analyzed by the power spectrum method described in section 4.3.2. Electrophoresis measurements were taken as a function of the applied (AC) electric-field frequency near the optical trapping corner frequency with trapping power $\approx 10mW$. Figure 7.2 displays the PSD response for electric-field frequencies ranging from $18Hz$ to $118Hz$ in increments of $10Hz$.

At each frequency increment, one dataset consisting of four data runs was acquired at a sampling frequency of $10kHz$ (2^{18} samples pre data run), and one data run was acquired in the absence of the electric-field before and after each electrophoresis dataset. Over the four data runs for each electrophoretic frequency the displacement response was binned (windowed) to eliminate noise, averaged, and plotted (colored lines) in Figure 7.2.

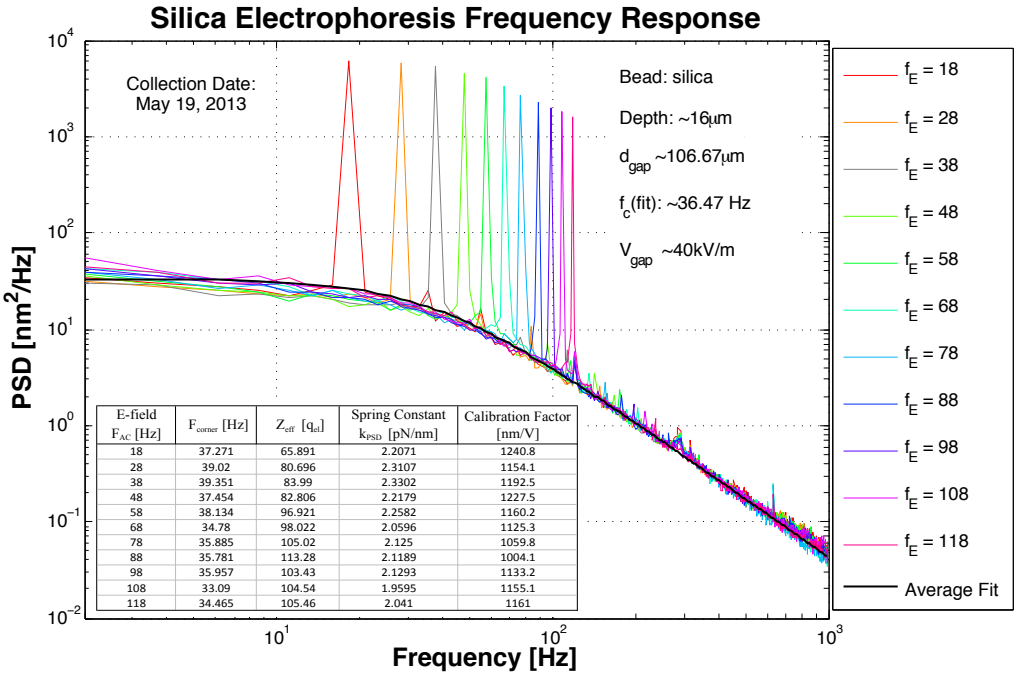

E-field F_{AC} [Hz]	F_{corner} [Hz]	Z_{eff} [q_{el}]	Spring Constant k_{PSD} [pN/nm]	Calibration Factor [nm/V]
18	37.271	65.891	2.2071	1240.8
28	39.02	80.696	2.3107	1154.1
38	39.351	83.99	2.3302	1192.5
48	37.454	82.806	2.2179	1227.5
58	38.134	96.921	2.2582	1160.2
68	34.78	98.022	2.0596	1125.3
78	35.885	105.02	2.125	1059.8
88	35.781	113.28	2.1189	1004.1
98	35.957	103.43	2.1293	1133.2
108	33.09	104.54	1.9595	1155.1
118	34.465	105.46	2.041	1161

Figure 7.2: Power spectral density of the electric-field frequency (f_{AC}) response for silica microspheres dispersed in de-ionized water. Each electrophoretic responses (colored lines) were averaged over four data runs, and a non-linear regression (Average fit) was fit.

Results and Discussion

The PSD responses in Figure 7.2 exhibit peak-like trends corresponding to the frequency of the applied electric-field, which is in agreement with Eqn. (7.4), the expected response. For each frequency dependent electrophoresis experiment the PSD response was fit with a Lorentzian and the corner frequency (trap stiffness) was extracted. The fit was subtracted from the experimental data and the remaining contributions was integrated over all frequencies. From the integration value, γ^2 was determined and the effective surface charge Z_eff was calculated through Eqn. (7.3). The calculated effective surface charge value corresponding to each electric-field frequency is presented in the table inset of Figure 7.2 and in Appendix A.3.

For this particular experiment, values for the effective surface charge Z_{eff} range from $\approx 66q_{el} - 113q_{el}$. These values are an order of magnitude larger than experiments involving PMMA microspheres in low dielectric suspension, dodecane ($\epsilon = 2$) [8, 9, 33]. However, similar electrophoretic experiments [34] involving deionized water have measured the effective surface charge of silica within a range of $\approx 471q_{el} - 2200q_{el}$. Discrepancies between [34] and the results presented in this section is most likely due to two assumption made for determining the effective surface charge. (1) The electric-field at the particle surface is approximately $E = V/d$, which is not the case because the dielectric constant of water ($\epsilon = 80$) was not taken into consideration. (2) Each computation is based on a model that assumes the Huckel limiting case, which does not account for nonlinear double layer relaxation effects.

Summary

The preliminary work presented in this section has accomplished the goals set-forth to instill supporting evidence that the experimental setup is capable of detecting and measuring electrophoretic effects. From these results we (OPE) now have a control to test the effects of monolayer coated silica spheres. Particularly, organic coating such as ADT-TES-F, an anthradithiophene (ADT) derivative functionalized with triethylsilylethynyl (TES) and fluorinated (F) side groups. Pending on the results of coated spheres, further electrophoretic experiments will be tweaked to investigate the charging nature. Such as, the charge in nonpolar liquid and adopting similar methods of [9] to analyze the discrete charging nature of each coating.

Experiments may include surface charge measurements and the dependence on the surrounding environment. That is, creating a more/less viscus, or polar liquid suspension and exploring how particular organic coatings respond to these changes. This approach may hold potential to pioneer a method for analyzing charge carrier dynamics of specific organic molecules and mechanisms involved with sub-elementary charge q_{el} resolution.

Appendix A

Additional Material

A.1 Optical Tweezer Setup

Optical Tweezer Setup Picture

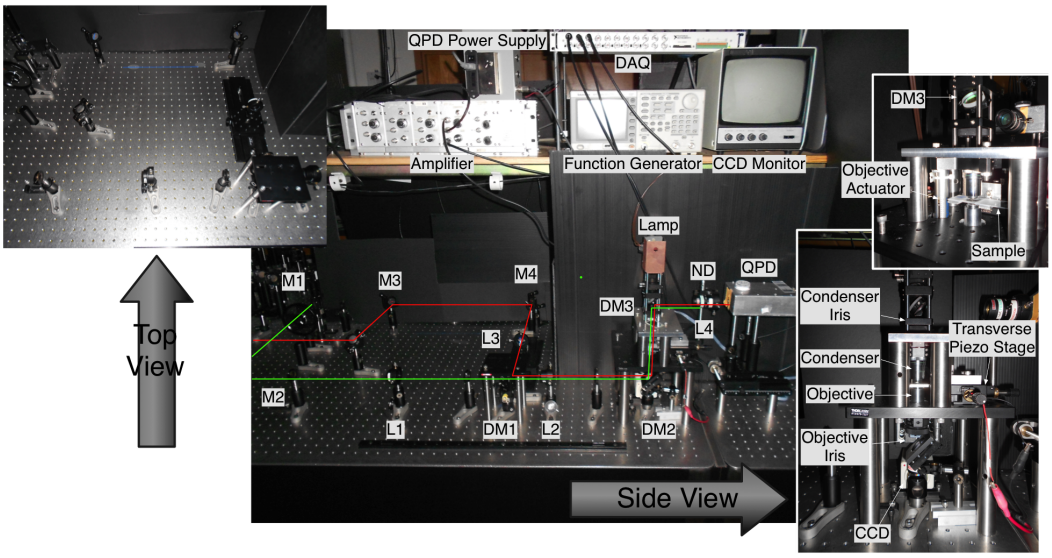

Figure A.1: Picture of the optical tweezer setup constructed including all active components

Figure A.1 displays the optical tweezer setup constructed and used for the work in this thesis. The following list of active components were used:

- Trapping laser IR (green): Mini ti:sapphire 800nm
- Detection laser He-Ne (red): Low powered 633nm
- M(x): Silver mirrors
- L1 and L2: Thor LA1608-B 75mm
- L3: 100nm doublet
- L4: Pcx1303 50mm
- DM1: 660DCLP

- DM2: Thor 43955
- DM3: Newport 05B20UF.25
- ND: E640SP and Thor FES0650
- Objective: 100/1.25 oil 160/0.17
- Condenser: Edmund DIN 20 0.40
- DAQ: National Instruments NI-6221
- CCD: Marshall V-1050A
- Transcoder Mike and Controller: ORIEL 18011 Encoder mike controller
- Function generator: Tektronix AFG 3021
- Custom build quadrant photodiode detector QPD (Mark Kendrick and Mark Warner)
- Custom LabVIEW acquisition program (not shown, Mark Kendrick 2007)
- Custom Mathematica data analysis program (not shown, Dr. David Mcintyre)

A.2 Force Measurements

This sections contains some supporting material corresponding to Chapter 4.

A.2.1 One-sided PSD constant G_o

The relation shown in this section corresponds to Einstein's diffusion constant and how it relate a Brownian particle's random thermal fluctuations to its mobility. This essentially relates fluctuation quantities and dissipation, which is also known as *fluctuating dissipation theory*, refer to [29] for more information on this topic.

The following relation is based from the writings of *Thermal cantilever calibration* by W. Trevor King [35].

Prelude

This relation utilizes the following Fourier transform properties and theorems [28].

Equipartition theorem:

$$\frac{1}{2}k_bT = \frac{1}{2}k_{trap}\langle x(t)\rangle^2 \tag{A.1}$$

where $\langle\ \rangle$ denotes the variance. Fourier transform normalization:

$$\mathcal{F}_f\{x(t)\}(f) \equiv \int_{-\infty}^{\infty} x(t)e^{-i2\pi\ ft}dt \tag{A.2}$$

Fourier property:

$$\mathcal{F}\left(\frac{d^nx(t)}{dt^n}\right) = (i2\pi f)^n\,\tilde{x}(f) \tag{A.3}$$

Parseval's theorem:

$$\int_{-\infty}^{\infty}|f(x)|^2dx = int_{-\infty}^{\infty}|\tilde{f}(k)|^2dk \tag{A.4}$$

We can translate Eqn. (A.2) to the one-sided power spectral density per unit time PSD:

$$PSD_f(x,f) \equiv \lim_{t_T\to\infty} \frac{1}{t_T} 2|\mathcal{F}_f\{x(t)\}(f)|^2 \tag{A.5}$$

where t_T is the total time for the acquired data. This relates to the variance of $x(t)$ through Parseval's theorem;

$$\langle x(t)^2\rangle = \int_0^\infty PSD_f(x,f)df \tag{A.6}$$

One-sided thermal PSD constant per unit time G_o

For the highly damped case, mapping the Langevin equation of motion into the frequency domain via Fourier transform yields;

$$F_B(t) = \beta\frac{dx}{dt} + k_{trap}x(t) \quad \xrightarrow{\mathcal{F}} \quad \tilde{F}_B(f) = (i\beta 2\pi f + k_{trap})\tilde{x}(f), \tag{A.7}$$

and taking the square complex norm of Eqn (A.7) and solving for $|\tilde{x}(f)|^2$;

$$|\tilde{F}_B(f)|^2 = (\beta^2 4\pi^2 f^2 + k^2)|\tilde{x}(f)|^2 \tag{A.8}$$

$$\Rightarrow \quad |\tilde{x}(f)|^2 = \frac{|\tilde{F}_B(f)|^2}{(2\pi\beta f)^2 + k_{trap}^2}. \tag{A.9}$$

Computing the PSD by inserting Eqn. (A.9) into Eqn. (A.5) gives the one-sided thermal power spectral density constant G_o per unit time;

$$PSD_f(\tilde{f}_B, f) = G_o = \lim_{t_T\to\infty} \frac{1}{t_T} 2|\tilde{f}_B(t)|^2 \tag{A.10}$$

Inserting Eqn. (A.10) into Eqn. (A.9) gives;

$$PSD(x,f) = \frac{G_o}{(2\pi\beta f)^2 + k_{trap}^2}. \tag{A.11}$$

Integrating Eqn. (A.11) over all positive frequencies gives the total power per

unit time;

$$\int_0^\infty PSD(x,f)df = \int_0^\infty \frac{G_o}{\beta^2 4\pi^2 f^2 + k_{trap}^2)} = \frac{G_o}{4\beta k_{trap}} \tag{A.12}$$

Now inserting this into Parseval's theorem relating the variance Eqn. (A.6) gives;

$$\langle x(t)^2 \rangle = \int_0^\infty PSD_f(x,f)df = \frac{G_o}{4\beta k_{trap}} \tag{A.13}$$

$$\Rightarrow \quad \langle x(t)^2 \rangle = \frac{G_o}{4\beta k_{trap}} \tag{A.14}$$

Relating the variance in Eqn. (A.14) with the equipartition theorem Eqn. (A.1) gives;

$$\langle x(t)^2 \rangle = \frac{k_B T}{k_{trap}} = \frac{G_o}{4\beta k_{trap}} \tag{A.15}$$

$$\Rightarrow \quad \boxed{G_o = 4\beta k_B T} \tag{A.16}$$

A.3 Surface Charge Measurements

Effective Surface Charge of Silica

E-field F_{AC} [Hz]	F_{corner} [Hz]	Z_{eff} [q_{el}]	Spring Constant k_{PSD} [pN/nm]	Calibration Factor [nm/V]
18	37.271	65.891	2.2071	1240.8
28	39.02	80.696	2.3107	1154.1
38	39.351	83.99	2.3302	1192.5
48	37.454	82.806	2.2179	1227.5
58	38.134	96.921	2.2582	1160.2
68	34.78	98.022	2.0596	1125.3
78	35.885	105.02	2.125	1059.8
88	35.781	113.28	2.1189	1004.1
98	35.957	103.43	2.1293	1133.2
108	33.09	104.54	1.9595	1155.1
118	34.465	105.46	2.041	1161

Table A.1: Effective surface charge of $1\mu m$-diameter silica spheres dispersed in water. Experiments were conducted at a trapping depth of $\approx 16\mu m$ from the cover-slip with laser trapping power $\approx 10mW$. The electrode separation was measured to be $\approx 106.6\mu m$ with an estimated electric-field strength of $E = V/d \approx 40kV/m$ resulting in the listed corner frequencies f_c, trapping spring constants k_{PSD}, calibration factor $cal = 1/\rho$, and effective surface charge Z_{eff} holding units of elementary charge q_{el}.

Comments

As mentioned at the end of chapter 7, there are other methods besides [8] that have been developed and critique in more recent years. The work of Semenov *et al.* [10] have been exploring the effects of both electrophoresis and electroosmosis in colloidal systems. Their method is similar to [8], in that the maximal displacement amplitude induced by the electric-field is linearly proportional to the electrophoretic mobility.

The collaborative work between Strubbe and Beunis *et al.* [9, 33, 36, 37] have provided a particularly interesting method that is capable of measuring the discrete dynamics of elementary charge. This method uses a data-windowing technique with sub-sampling frequencies larger than the observed

charging cycles. In turn, the discrete nature of single charging events q_{el} near the particle surface is measured.

These measurements are rather simple, based upon a high (AC) electric-field frequency and utilizing a weighted sum of the two-sided PSD during each sampling window. The main benefit of this method is (1) rapid sampling frequency provide bare surface charge measurements (not effective), (2) analysis of the two-sided PSD preserves the *sign* of charge measurements, and (3) measurements are capable of resolving discrete, elementary charging events, that is, the error in each windowing measurement is smaller than the magnitude of an electron charge q_{el}. Preliminary experiments utilizing this technique have been implemented involving non-coated silica spheres, which yield promising results, and further experiments are being considered.

Further Interests

- Explore the techniques developed in [9] for silica in nonpolar liquid
- Begin analyzing coated silica spheres
- Explore the electric field dependence at high frequencies using [9]
- Explore the possibilities of adding a band-pass filter to eliminate external frequency noise
- Measure electroosmosis in differing frequency regimes
- incorporate a modulated signal to sweep through certain regions of frequencies
- Determine the trapping power need to minimize low frequency lag contributions
- Add a DC filter to amplifier

Bibliography

[1] Stephen R Forrest. The path to ubiquitous and low-cost organic electronic appliances on plastic. *Nature*, 428(6986):911–918, 2004.

[2] Christos D Dimitrakopoulos and Patrick RL Malenfant. Organic thin film transistors for large area electronics. *Advanced Materials*, 14(2):99–117, 2002.

[3] Tommie W Kelley, Paul F Baude, Chris Gerlach, David E Ender, Dawn Muyres, Michael A Haase, Dennis E Vogel, and Steven D Theiss. Recent progress in organic electronics: Materials, devices, and processes. *Chemistry of Materials*, 16(23):4413–4422, 2004.

[4] Arthur Ashkin. Acceleration and trapping of particles by radiation pressure. *Physical review letters*, 24(4):156–159, 1970.

[5] Arthur Ashkin. History of optical trapping and manipulation of small-neutral particle, atoms, and molecules. *Selected Topics in Quantum Electronics, IEEE Journal of*, 6(6):841–856, 2000.

[6] Steven M Block. Nanometres and piconewtons: the macromolecular mechanics of kinesin. *Trends in cell biology*, 5(4):169–175, 1995.

[7] Giuseppe Pesce, Biagio Mandracchia, Emanuele Orabona, Giulia Rusciano, Luca De Stefano, and Antonio Sasso. Mapping electric fields generated by microelectrodes using optically trapped charged microspheres. *Lab on a Chip*, 11(23):4113–4116, 2011.

[8] G Seth Roberts, Tiffany A Wood, William J Frith, and Paul Bartlett. Direct measurement of the effective charge in nonpolar suspensions by optical tracking of single particles. *The Journal of chemical physics*, 126(19):194503–194503, 2007.

[9] Filip Beunis, Filip Strubbe, Kristiaan Neyts, and Dmitri Petrov. Beyond millikan: the dynamics of charging events on individual colloidal particles. *Physical review letters*, 108(1):016101, 2012.

[10] I Semenov, O Otto, G Stober, P Papadopoulos, UF Keyser, and F Kremer. Single colloid electrophoresis. *Journal of colloid and interface science*, 337(1):260–264, 2009.

[11] Arthur Ashkin, JM Dziedzic, JE Bjorkholm, and Steven Chu. Observation of a single-beam gradient force optical trap for dielectric particles. *Optics letters*, 11(5):288–290, 1986.

[12] Keir C Neuman and Steven M Block. Optical trapping. *Review of scientific instruments*, 75(9):2787–2809, 2004.

[13] MJ Kendrick, DH McIntyre, and O Ostroverkhova. Wavelength dependence of optical tweezer trapping forces on dye-doped polystyrene microspheres. *JOSA B*, 26(11):2189–2198, 2009.

[14] Josep Mas, Arnau Farré, Jordi Cuadros, Ignasi Juvells, and Artur Carnicer. Understanding optical trapping phenomena: A simulation for undergraduates. *Education, IEEE Transactions on*, 54(1):133–140, 2011.

[15] Mark J Kendrick. *Light-matter interactions: from the photophysics of organic semiconductors to high spatial resolution optical tweezer-controlled nanoprobes*. PhD thesis, Oregon State University, 2012.

[16] Maria Dienerowitz, Michael Mazilu, and Kishan Dholakia. Optical manipulation of nanoparticles: a review. *Journal of Nanophotonics*, 2(1):021875–021875, 2008.

[17] David Jeffrey Griffiths and Reed College. *Introduction to electrodynamics*, volume 3. prentice Hall New Jersey, 1999.

[18] Interactive simulations: University of colorado at boulder optical tweezers and applications, November 2011.

[19] Aruna Ranaweera. *Investigations with Optical Tweezers: Construction, Identification, and Control*. PhD thesis, University of California Santa Barbara, September 2004.

[20] Albert Einstein. The theory of the brownian movement. *Ann. der Physik*, 17:549, 1905.

[21] Ming Chen Wang and George Eugène Uhlenbeck. On the theory of the brownian motion ii. *Reviews of Modern Physics*, 17(2-3):323–342, 1945.

[22] George E Uhlenbeck and Leonard Salomon Ornstein. On the theory of the brownian motion. *Physical review*, 36(5):823, 1930.

[23] Don S Lemons and Anthony Gythiel. Paul langevin's 1908 paper "on the theory of brownian motion"["sur la théorie du mouvement brownien," cr acad. sci.(paris)[bold 146], 530–533 (1908)]. *American Journal of Physics*, 65:1079, 1997.

[24] Tutorials: Optical trapping lab.

[25] E-L Florin, A Pralle, EHK Stelzer, and JKH Hörber. Photonic force microscope calibration by thermal noise analysis. *Applied Physics A: Materials Science & Processing*, 66:S75–S78, 1998.

[26] David H. Mcintyre. *Quantum Mechanics: A Paradigms Approach*. Pearson, 2012.

[27] Kirstine Berg-Sørensen and Henrik Flyvbjerg. Power spectrum analysis for optical tweezers. *Review of Scientific Instruments*, 75(3):594–612, 2004.

[28] K Kenneth Franklin Riley, M Michael Paul Hobson, and S Stephen John Bence. *Mathematical methods for physics and engineering*. Cambridge University Press, 2006.

[29] Rep Kubo. The fluctuation-dissipation theorem. *Reports on Progress in Physics*, 29(1):255, 1966.

[30] Mark C Williams. Optical tweezers: measuring piconewton forces. *Biophysics Textbook Online: http://www. biophysics. org/btol*, 2002.

[31] Karel Svoboda and Steven M Block. Biological applications of optical forces. *Annual review of biophysics and biomolecular structure*, 23(1):247–285, 1994.

[32] Kirstine Berg-Sørensen, Erwin JG Peterman, Tom Weber, Christoph F Schmidt, and Henrik Flyvbjerg. Power spectrum analysis for optical tweezers. ii: Laser wavelength dependence of parasitic filtering, and how to achieve high bandwidth. *Review of scientific instruments*, 77(6):063106–063106, 2006.

[33] Filip Strubbe, Filip Beunis, and Kristiaan Neyts. Detection of elementary charges on colloidal particles. *Physical review letters*, 100(21):218301, 2008.

[34] Sven H Behrens and David G Grier. The charge of glass and silica surfaces. *Journal of chemical physics*, 115(14):6716–6721, 2001.

[35] W. Trevor King. Thermal cantilever calibration. October 2009.

[36] Filip Beunis, Filip Strubbe, Bart Verboven, Kristiaan Neyts, and Dmitri Petrov. Fast and precise measurements of particle charge with optical trapping electrophoresis. In *OPTO*, pages 76130B–76130B. International Society for Optics and Photonics, 2010.

[37] Filip Strubbe, Filip Beunis, and Kristiaan Neyts. Determination of the effective charge of individual colloidal particles. *Journal of colloid and interface science*, 301(1):302–309, 2006.